



# Photonics-based MIMO radar with high-resolution and fast detection capability

FANGZHENG ZHANG,<sup>1</sup> BINDONG GAO,<sup>1</sup> AND SHILONG PAN<sup>1,\*</sup>

College of Electronic and Information Engineering, Nanjing University of Aeronautics and Astronautics, Nanjing 210016, China

\*pans@nuaa.edu.cn

**Abstract:** A photonics-based multiple-input-multiple-output (MIMO) radar is proposed and demonstrated based on wavelength-division-multiplexed broadband microwave photonic signal generation and processing. The proposed radar has a large operation bandwidth, which helps to achieve an ultra-high range resolution. Compared with a monostatic radar, improved radar performance and extended radar applications originated from the MIMO architecture can be achieved. In addition, low-speed electronics with real-time signal processing capability is feasible. A photonics-based  $2 \times 2$  MIMO radar is established with a 4-GHz bandwidth in each transmitter and a sampling rate of 100 MSa/s in the receiver. Performance of the photonics-based multi-channel signal generation and processing is evaluated, and an experiment for direction of arrival (DOA) estimation and target positioning is demonstrated, through which the feasibility of the proposed radar system can be verified.

© 2018 Optical Society of America under the terms of the [OSA Open Access Publishing Agreement](#)

**OCIS codes:** (060.5625) Radio frequency photonics; (350.4010) Microwaves; (280.5600) Radar.

## References and links

1. M. I. Skolnik, *Radar Handbook* (McGraw-Hill, 2008).
2. P. Ghelfi, F. Laghezza, F. Scotti, G. Serafino, S. Pinna, D. Onori, E. Lazzeri, and A. Bogoni, "Photonics in radar systems," *IEEE Microw. Mag.* **16**(8), 74–83 (2015).
3. D. Grodensky, D. Kravitz, and A. Zadok, "Ultra-wideband microwave-photonic noise radar based on optical waveform generation," *IEEE Photonics Technol. Lett.* **24**(10), 839–841 (2012).
4. P. Ghelfi, F. Laghezza, F. Scotti, G. Serafino, A. Capria, S. Pinna, D. Onori, C. Porzi, M. Scaffardi, A. Malacarne, V. Vercesi, E. Lazzeri, F. Berizzi, and A. Bogoni, "A fully photonics-based coherent radar system," *Nature* **507**(7492), 341–345 (2014).
5. W. Zou, H. Zhang, X. Long, S. Zhang, Y. Cui, and J. Chen, "All-optical central-frequency-programmable and bandwidth-tailorable radar," *Sci. Rep.* **6**(1), 19786 (2016).
6. F. Zhang, Q. Guo, and S. Pan, "Photonics-based real-time ultra-high-range-resolution radar with broadband signal generation and processing," *Sci. Rep.* **7**(1), 13848 (2017).
7. R. Li, W. Li, M. Ding, Z. Wen, Y. Li, L. Zhou, S. Yu, T. Xing, B. Gao, Y. Luan, Y. Zhu, P. Guo, Y. Tian, and X. Liang, "Demonstration of a microwave photonic synthetic aperture radar based on photonic-assisted signal generation and stretch processing," *Opt. Express* **25**(13), 14334–14340 (2017).
8. Y. Tong, D. Han, R. Cheng, Z. Liu, W. Xie, J. Qin, and Y. Dong, "Photonics-based coherent wideband linear frequency modulation pulsed signal generation," *Opt. Lett.* **43**(5), 1023–1026 (2018).
9. S. Peng, S. Li, X. Xue, X. Xiao, D. Wu, X. Zheng, and B. Zhou, "High-resolution W-band ISAR imaging system utilizing a logic-operation-based photonic digital-to-analog converter," *Opt. Express* **26**(2), 1978–1987 (2018).
10. Y. Yao, F. Zhang, Y. Zhang, X. Ye, D. Zhu, and S. Pan, "Demonstration of ultra-high-resolution photonics-based Ka-band inverse synthetic aperture radar imaging," in *2018 Optical Fiber Communication Conference (OFC, 2018)*, paper Th3G.5.
11. F. Zhang, Q. Guo, Z. Wang, P. Zhou, G. Zhang, J. Sun, and S. Pan, "Photonics-based broadband radar for high-resolution and real-time inverse synthetic aperture imaging," *Opt. Express* **25**(14), 16274–16281 (2017).
12. F. Zhang, Q. Guo, Y. Zhang, Y. Yao, P. Zhou, D. Zhu, and S. Pan, "Photonics-based real-time and high-resolution ISAR imaging of non-cooperative target," *Chin. Opt. Lett.* **15**(11), 112801 (2017).
13. O. Aldayel, V. Monga, and M. Rangaswamy, "Tractable transmit MIMO beampattern design under a constant modulus constraint," *IEEE Trans. Signal Process.* **65**(10), 2588–2599 (2017).
14. C. Ma, T. S. Yeo, Y. Zhao, and J. Feng, "MIMO radar 3D imaging based on combined amplitude and total variation cost function with sequential order one negative exponential form," *IEEE Trans. Image Process.* **23**(5), 2168–2183 (2014).
15. T. Yao, D. Zhu, D. Ben, and S. Pan, "Distributed MIMO chaotic radar based on wavelength-division multiplexing technology," *Opt. Lett.* **40**(8), 1631–1634 (2015).

16. H. Yang and J. Chun, "An improved algebraic solution for moving target localization in noncoherent MIMO radar systems," *IEEE Trans. Signal Process.* **64**(1), 258–270 (2016).
17. I. Bekkerman and J. Tabrikian, "Target detection and localization using MIMO radars and sonars," *IEEE Trans. Signal Process.* **54**(10), 3873–3883 (2006).
18. J. Li and P. Stoica, "MIMO radar with collocated antennas," *IEEE Signal Process. Mag.* **24**(5), 106–114 (2007).
19. Q. Guo, F. Zhang, P. Zhou, and S. Pan, "Dual-band LFM signal generation by frequency quadrupling and polarization multiplexing," *IEEE Photonics Technol. Lett.* **29**(16), 1320–1323 (2017).
20. H. Messer, G. Signal, and L. Bialy, "On the achievable DF accuracy of two kinds of active interferometers," *IEEE Trans. Aerosp. Electron. Syst.* **32**(3), 1158–1164 (1996).
21. S. Rao, "MIMO Radar," Texas Instruments Application Report **SWRA554**, 1–12 (2017).
22. K. Xu, X. Sun, J. Yin, H. Huang, J. Wu, X. Hong, and J. Lin, "Enabling ROF technologies and integration architectures for in-building optical–wireless access networks," *IEEE Photonics J.* **2**(2), 102–112 (2010).
23. D. Marpaung, C. Roeloffzen, R. Heideman, A. Leinse, S. Sales, and J. Capmany, "Integrated microwave photonics," *Laser Photonics Rev.* **7**(4), 506–538 (2013).

## 1. Introduction

Radar is widely used in both civil and security applications. With the increasing requirement for high-resolution target detection and imaging, broadband radars are highly demanded to achieve a high range resolution [1, 2]. To overcome the bandwidth limitations of traditional radar transmitters and receivers, microwave photonic technologies have been applied to construct broadband radars with an ultra-high range resolution [3–9]. In [6], we have proposed a high-range-resolution radar based on photonic generation and processing of broadband linear frequency modulation (LFM) signals. In this system, the broadband LFM signal is generated by photonic frequency quadrupling, and the received radar echo is de-chirped by photonic frequency mixing. This photonics-based radar has a potential bandwidth of tens of gigahertz, enabling an ultra-high range resolution. Besides, the photonics-based broadband de-chirp processing transfers the target information from the radar echo to a low-frequency signal, which effectively reduces the required sampling rate of the digital receiver and ensures a fast or real-time signal processing. Based on this architecture, a Ka-band radar with a 12-GHz bandwidth is demonstrated with a range resolution as high as 1.3 cm [10]. Turntable inverse synthetic aperture radar (ISAR) imaging experiment is performed with a 2D imaging resolution of  $2\text{ cm} \times 2\text{ cm}$  [11], and real-time ISAR imaging of a non-cooperative target is also demonstrated [12]. These results can confirm the advantage of photonics-based broadband radar in achieving an ultra-high range resolution. However, the previous photonics-based radars are mainly focused on monostatic radar structures and applications. To further improve the radar performance, such as to achieve a higher azimuth resolution and more precise parameter estimation, and also to enable more radar applications such as direction of arrival (DOA) estimation and multiple target tracking, it is urgent to combine the photonics-based radar technology with the array radar technology. In recent years, multiple-input-multiple-output (MIMO) radar has been considered as a promising array radar architecture, which can have a large equivalent transceiver array with relaxed hardware requirements as compared with a conventional radar array. Thanks to its orthogonal property between different channels, a MIMO radar has the flexibility to realize multiple beam forming, DOA estimation, multiple target tracking, and 2D/3D imaging, etc [13–16]. In addition, a MIMO radar can achieve a high azimuth resolution and very precise target positioning and parameter estimation [17, 18]. Currently, the main difficulties in developing high-resolution MIMO radars are: i) the range resolution still suffers from the electronic bandwidth limitation; ii) the data storage and signal processing in multiple receivers is quite resource-consuming and complex, especially for broadband MIMO radar receivers where high-speed ADCs are usually applied. Although photonics-based radar has been demonstrated with great potential in future radar applications, the design of broadband MIMO radar based on photonic technologies has not been reported.

In this paper, we propose a photonics-based broadband MIMO radar, in which wavelength-division multiplexed microwave photonic signal generation and processing are adopted to achieve a large operation bandwidth and a simple echo de-chirping and separation.

In the transmitter array, multiple orthogonal LFM signals are generated by photonic frequency multiplication, and in the receiver array, de-chirping and separation of radar echoes from different channels are implemented by photonic frequency mixing. In addition to the large operation bandwidth originated from the photonics-based system and the various advantages originated from the MIMO radar, hardware requirements of the proposed photonics-based MIMO radar are also relaxed. In each transmitter, electrical signal generators with a moderate sampling rate are adequate to generate high-frequency and broadband LFM signals. In each receiver, low-speed analog-to-digital converters (ADCs) are sufficient to sample the de-chirped signals, and signal separation between different channels is implemented by the hardware instead of digital matched filters. In this work, principle of the proposed photonics-based MIMO radar is described in detail, and its feasibility is experimentally verified through a  $2 \times 2$  MIMO radar system with a 4-GHz bandwidth in each channel and a 100-MSa/s sampling rate in the receiver. Based on the established experimental system, performance of the photonics-based multi-channel signal generation and processing is evaluated, and DOA estimation and target positioning are also demonstrated.

## 2. Principle of the photonics-based MIMO radar

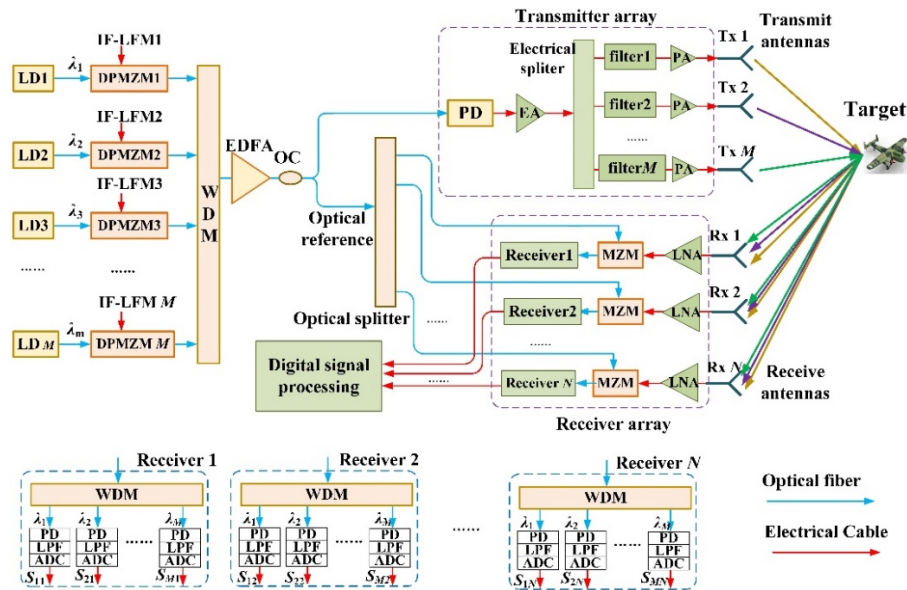


Fig. 1. Schematic diagram of the proposed photonics-based  $M \times N$  MIMO radar. LD: laser diode; OC: optical coupler; DPMZM: dual-parallel Mach-Zehnder modulator; WDM: wavelength division multiplexer; EDFA: erbium-doped fiber amplifier; PD: photodetector; EA: electrical amplifier; PA: power amplifier; LNA: low noise amplifier; MZM: Mach-Zehnder modulator; LPF: electrical low-pass filter; ADC: analog-to-digital converter.

Figure 1 shows the schematic diagram of the proposed photonics-based MIMO radar with  $M$ -transmitter and  $N$ -receiver, which is designed based on a wavelength division multiplexing architecture. Each transmitter generates an LFM signal in the form of either pulsed signal or continuous wave signal, and frequency overlap is avoided between adjacent transmitters, which guarantees the orthogonality of the transmitted signals. As shown in Fig. 1,  $M$  laser diodes (LDs) with different wavelengths ( $\lambda_1, \lambda_2, \dots, \lambda_M$ ) are used as the light sources. The light from each LD is modulated by a dual-parallel Mach Zehnder modulator (DPMZM) that is driven by an intermediate frequency LFM (IF-LFM) signal. The  $M$  orthogonal IF-LFM signals have the same bandwidth and chirp rate, and they are generated by signal generators such as a direct digital synthesizer. In the  $m^{\text{th}}$  channel ( $i = 1, 2, \dots, M$ ), the instantaneous frequency of a single LFM pulse is expressed as

$$f_{\text{IF}_m}(t) = u_m + kt \quad (0 \leq t \leq T) \quad (1)$$

where  $u_m$  is the initial frequency,  $T$  is the temporal width of the pulse, and  $k = B/T$  is the chirp rate with  $B$  being the signal bandwidth. To avoid frequency overlap between adjacent channels,  $u_{m+1} > f_m(T)$  should be satisfied. Each DPMZM is properly biased to operate at the frequency quadrupling mode, i.e., only the frequency sweeping  $\pm 2$ nd order sidebands are generated after modulating the input light [19]. The output signals of the DPMZMs are combined by a wavelength division multiplexer (WDM) and properly amplified by an erbium-doped fiber amplifier (EDFA). Then, the optical signal is split into two branches by an optical coupler (OC). The signal in the upper branch is sent to a broadband photodetector (PD) to implement optical-to-electrical conversion. After the PD,  $M$  LFM signals are generated with the instantaneous frequency of the  $m^{\text{th}}$  LFM signal expressed as

$$f_{\text{LFM}_m}(t) = 4u_m + 4kt \quad (0 \leq t \leq T) \quad (2)$$

Compared with the input IF-LFM signals, the frequency and bandwidth of the obtained LFM signals are quadrupled. In this process, to avoid the interference between different optical channels, the wavelength spacing between two adjacent light sources should be far larger than the bandwidth of the PD. The generated LFM signals are separated by a series of electrical filters with different central frequencies. Then, each LFM signal is amplified by a power amplifier (PA) and emitted to the air through a transmit antenna. The electromagnetic wave transmitted by the multiple antennas are scattered by the target, and the reflected echoes are collected by  $N$  receive antennas without signal selection. Then, de-chirp processing and signal separation between different channels are implemented utilizing the optical signal from the lower branch of the OC. This optical signal is split into  $N$  branches by an optical splitter to obtain  $N$  reference signals. The echo signal collected by a receive antenna is amplified by a low noise amplifier (LNA) and then applied to drive a Mach-Zehnder modulator (MZM) to perform intensity modulation of a reference optical signal from the optical splitter. After that, the modulated optical signal is sent to a receiver. In the  $n^{\text{th}}$  receiver ( $n = 1, 2, \dots, N$ ), the input optical signal passes through another WDM, which has the same transmission properties as used in the signal generation part, to perform wavelength de-multiplexing of the  $M$  optical channels. Each de-multiplexed optical signal is sent to a PD to implement de-chirping of the received LFM signals by microwave photonic frequency mixing. After the PD, an electrical low-pass filter (LPF) with a proper bandwidth is used to select out the de-chirped signal, which is then digitized by a low-speed ADC. In this way,  $M$  digital signals, corresponding to the de-chirped signals of the  $M$  orthogonal echoes, are separately obtained in each receiver. In Fig. 1, the signal  $S_{mn}$  represents the de-chirped signal originated from the  $m^{\text{th}}$  transmitter and received by the  $n^{\text{th}}$  receiver. Finally, the  $MN$  digital signals obtained by the receiver array are sent to a digital signal processing module.

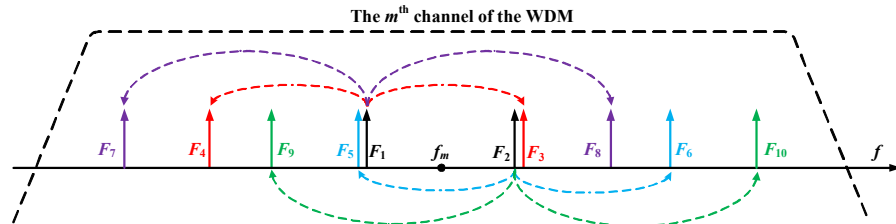


Fig. 2. Illustration of the optical spectrum in the  $m^{\text{th}}$  output channel of the WDM in a receiver.

In each receiver, to well separate the de-chirped signals from different channels, the multiple LFM signals transmitted by the MIMO radar should be properly designed. Figure 2 illustrates the optical spectrum of the signal after the MZM in the  $m^{\text{th}}$  output channel of the WDM, at time  $t$ . In this channel, the echo signal corresponding to the  $m^{\text{th}}$  transmitter is to be

de-chirped and selected. In Fig. 2,  $f_m$  is the frequency of the laser source with the wavelength of  $\lambda_m$ . The reference optical signal sent to the MZM can be treated as two frequency sweeping optical carriers at  $F_1 = f_m - 2u_m - 2kt$ , and  $F_2 = f_m + 2u_m + 2kt$ . The instantaneous frequency of the echo signal from the  $m^{\text{th}}$  transmitter is  $4u_m + 4k(t + \tau_m)$ , where  $\tau_m$  is the time delay of the echo signal. By controlling the modulation index, only the  $\pm 1$ st order sidebands with the optical carrier are obtained after the MZM. Thus, a pair of sidebands at  $F_3 = f_m + 2u_m + 2kt + 4k\tau_m$  and  $F_4 = f_m - 6u_m - 6kt - 4k\tau_m$ , and another pair of sidebands at  $F_5 = f_m - 2u_m - 2kt - 4k\tau_m$  and  $F_6 = f_m + 6u_m + 6kt + 4k\tau_m$  are generated. After the PD, the desired de-chirped signal at frequency  $\Delta f = 4k\tau_m$  is obtained by frequency beating between  $F_2$  and  $F_3$  (or between  $F_1$  and  $F_5$ ). Considering  $4k\tau_m$  is usually a small value, the de-chirped signal can be selected out by an LPF with a small bandwidth. It should be noted that the optical carriers at  $F_1$  and  $F_2$  are also intensity modulated by a signal at  $4u_{m+1} + 4k(t + \tau_{m+1})$ , which is the echo signal of the  $(m + 1)^{\text{th}}$  transmitter with  $\tau_{m+1}$  being the time delay. The generated  $\pm 1$ st order modulation sidebands, denoted by  $F_7, F_8, F_9$ , and  $F_{10}$ , are also shown in Fig. 2, where  $F_7 = f_m - 2u_m - 6kt - 4u_{m+1} - 4k\tau_{m+1}$ ,  $F_8 = f_m - 2u_m + 2kt + 4u_{m+1} + 4k\tau_{m+1}$ ,  $F_9 = f_m + 2u_m - 2kt - 4u_{m+1} - 4k\tau_{m+1}$ , and  $F_{10} = f_m + 2u_m + 6kt + 4u_{m+1} + 4k\tau_{m+1}$ . It is found that when the following conditions are satisfied,

$$4(u_{m+1} - u_m) \gg \Delta f \quad (3)$$

$$f_{\text{LFM}_m}(t) - 4(u_{m+1} - u_m) \gg \Delta f \quad (4)$$

all the frequencies generated by beating at the PD, except the desired de-chirped component, are far greater than  $\Delta f$ . Therefore, the de-chirped signal can be separated using an LPF without interference from the  $(m + 1)^{\text{th}}$  transmitter. In obtaining (3) and (4),  $\tau_m \approx \tau_{m+1}$  is assumed, because the target distance is greatly larger than the distance between adjacent transmit antennas or adjacent receive antennas. Equation (3) indicates that the initial frequency difference between adjacent channels should be far greater than the de-chirped frequency, which can be easily satisfied by choosing a signal bandwidth larger than  $\Delta f$ . For example, a radar with a bandwidth over 500 MHz is feasible when the de-chirped signal is kept within 100 MHz. Equation (4) requires that frequency of the radar signal should be greatly larger than the initial frequency difference between adjacent channels. This is also easy to implement, e.g., when the frequency difference between adjacent channels is no more than 5 GHz, a MIMO radar operating over 5.5 GHz can well separate the de-chirped signals without interference from adjacent channels. Although Fig. 2 only includes the frequency components caused by the most adjacent channel, further investigation confirms that the de-chirped signal at  $\Delta f$  can be separated without interference from all the other channels when (3) and (4) are satisfied, as long as all the transmitters have the same bandwidth and chirp rate.

To this point, explanation of the photonics-based MIMO radar structure is completed. Advantages of the proposed system are attributed to the combination of microwave photonic technology and MIMO radar technology. Firstly, a large operation bandwidth is enabled by the photonics-based broadband signal generation and de-chirp processing, leading to a high radar range resolution. Secondly, thanks to the MIMO radar architecture, improved radar detection performance (such as a higher azimuth resolution and more precise parameter estimation) and extended radar applications (such as multiple targets detection and multiple beamforming, etc.) can be achieved compared with a monostatic radar. Thirdly, low-speed electronics with real-time signal processing capability is feasible in the proposed radar. In the transmitters, electrical signal generators with moderate sampling rate can be used to generate high-frequency and broadband LFM signals. In each receiver, a low-speed ADC is required to sample the de-chirped signal and separation of the de-chirped signal is realized by hardware instead of conventional digital matched filters, which can lower the requirement for data storage and increase the signal processing speed.

### 3. Experimental demonstration

To verify the feasibility of the proposed radar system, a  $2 \times 2$  MIMO radar is established based on the experimental setup in Fig. 3. Due to the hardware constraints, the two receiving channels share the same receiver in a time-division mode after collecting the echoes by the two receive antennas. Although this configuration only permits the observation of static targets, it does not affect the performance evaluation of the photonic system.

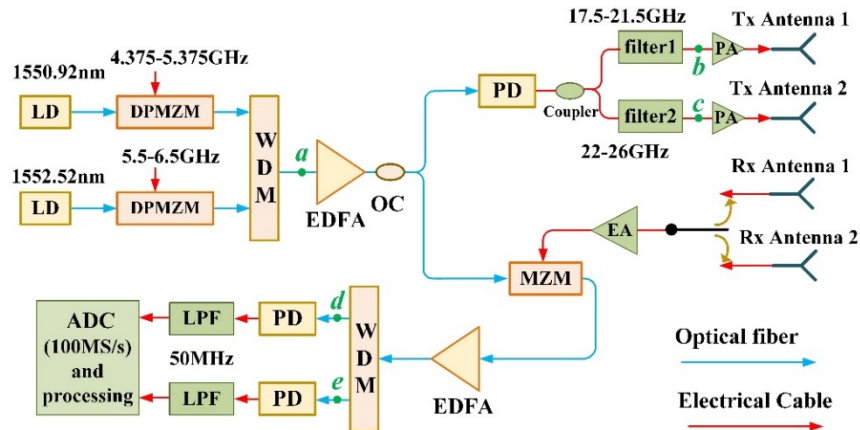


Fig. 3. Experimental setup of the photonics-based  $2 \times 2$  MIMO radar.

In Fig. 3, two LDs at 1550.92 nm and 1552.52 nm (separated by 200 GHz), both with an output power of 16 dBm are used as the light sources. The output light from each LD is modulated by a DPMZM (Fujitsu FTM7962EP, Bandwidth: 22 GHz), respectively. The two IF-LFM signals driving the two DPMZMs are generated by a two-channel arbitrary waveform generator (Keysight 8195A), and both of them have a repetition rate of 100 kHz and a bandwidth of 1 GHz (4.375-5.375 GHz and 5.5-6.5 GHz, respectively). After properly setting the bias voltages of the DPMZMs, frequency quadrupling modulation can be achieved. The obtained two optical signals are combined by a WDM that has a channel spacing of 100 GHz. Figure 4 shows the optical spectrum of the signal after the WDM (point *a* in Fig. 3), which is measured by an optical spectrum analyzer (Yokogawa AQ6370C) with a resolution of 0.02 nm. As can be seen, for both of the two optical channels, two frequency-swept  $\pm 2$ nd-order optical sidebands are generated with the undesired sidebands well suppressed. This optical signal is amplified by an EDFA (Amonics Ltd.) with a gain of about 20 dB. Then, a 50:50 OC is used to equally split the optical signal. The signal from the upper branch is sent to a 40-GHz PD (u2t XPDV2120RA). After the PD, two LFM signals covering 17.5-21.5 GHz and 22-26 GHz are generated, and two electrical band-pass filters are applied to separate the two LFM signals. Waveforms of the generated two LFM signals in a period of 40  $\mu$ s are observed by an 80-GSa/s real-time oscilloscope (Keysight DSO-X 92504A), as shown in Figs. 5(a) and 5(c). The corresponding electrical spectra are measured (point *b* and point *c* in Fig. 3) by an electrical spectrum analyzer (ESA, R&S FSV40) with a resolution bandwidth (RBW) of 50 kHz, as shown in Figs. 5(b) and 5(d), respectively. As can be seen, two 4-GHz bandwidth LFM signals covering 17.5-21.5 GHz and 22-26 GHz are successfully generated, confirming the multi-channel broadband signal generation capability of the proposed system. The In-band signal-to-noise and distortion ratio (SINAD) of the two LFM signals is also measured by the ESA with an RBW of 10 Hz, which is 59 dB and 58 dB, respectively. The generated two LFM signals are amplified individually by a broadband electrical amplifier (Agilent 87422A), and launched into the air by two K-band antennas respectively. The transmitted power by each antenna is about 0.5 W.

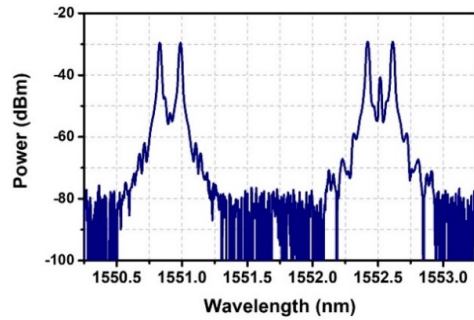


Fig. 4. Spectra of the frequency quadrupling modulated optical signal after the WDM (measured at point *a* in Fig. 3).

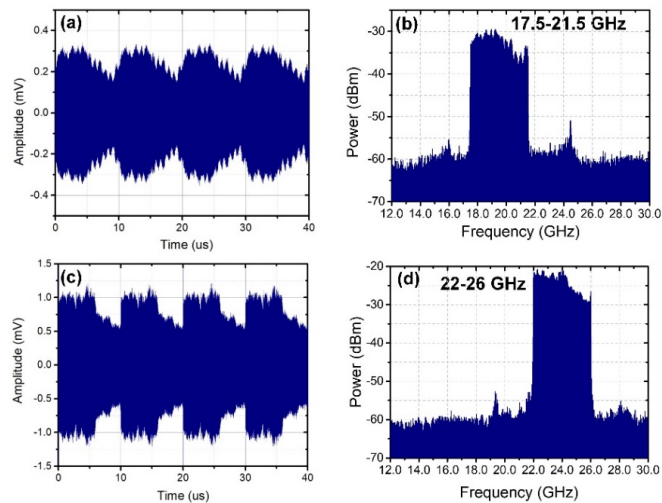


Fig. 5. (a) Waveform and (b) spectrum of the generated LFM signal in 17.5-21.5 GHz (RBW = 50 kHz, measured at point *b* in Fig. 3); (c) waveform and (d) spectrum of the generated LFM signal in 22-26 GHz (RBW = 50 kHz, measured at point *c* in Fig. 3).

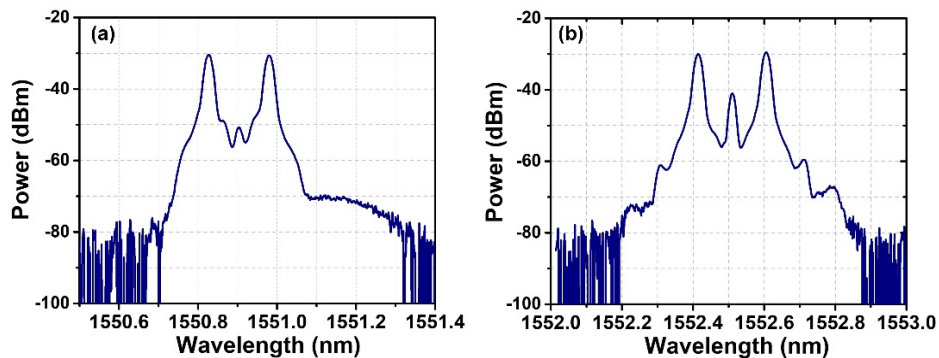


Fig. 6. Spectra of the de-multiplexed two optical signals after the WDM in the receiver: (a) the 1550.92 nm channel and (b) the 1552.52 nm channel (measured at point *d* and point *e* in Fig. 3, respectively).

To check the feasibility of the multi-channel de-chirping and signal separation, a distance measurement experiment is implemented applying the two transmitters and a single receiver. In this case, a simple linear antenna distribution is adopted, where the two transmit antennas and the receive antenna are close to one another with the receive antenna placed in the middle. A metallic plane target with a size of about  $6\text{ cm} \times 4\text{ cm}$  is placed at a distance of 160.9 cm away from the antennas. The radar echo is collected by the receive antenna and amplified by a broadband electrical amplifier (SHF 806E). The obtained signal is applied to drive an MZM (Fujitsu FTM7938, Bandwidth: 28 GHz). The output signal from the MZM is amplified by another EDFA and sent to a WDM to implement wavelength de-multiplexing. Figure 6 (a) and (b) show the spectra of the de-multiplexed two optical signals (point *d* and point *e* in Fig. 3). Then, the two signals are sent to a PD (CONQUER Inc., Bandwidth: 10GHz) respectively. Following each PD, an LPF with a bandwidth of 50 MHz is used to select the de-chirped signal. The obtained two de-chirped signals are simultaneously sampled by two channels of the real-time oscilloscope, both with a sampling rate of 100 MSa/s. Figures 7(a) and 7(c) show the raw data of the sampled two de-chirped signals ( $S_{11}$  and  $S_{21}$ ) in a period of 100  $\mu\text{s}$ . By performing fast Fourier transformation (FFT) to the two signals, the electrical power spectra are obtained, as shown in Figs. 7(b) and 7(d), respectively. As can be seen, two strong frequency components at 9.9 MHz and 16.19 MHz are observed, corresponding to the de-chirped frequency components in the two channels, respectively. Here, normalized power spectra are provided. The specific power level of the two de-chirped frequency components is measured to be around  $-40\text{ dBm}$ . Through the spectra in Fig. 7, it is also found that, the de-chirped signals of the two channels are successfully separated without interference between each other. To acquire the correct information through the calculated spectra in Fig. 7, a calibration should be implemented to remove the de-chirped frequency shift due to time delay of the electrical cables and other devices, such that the de-chirped frequency is proportional to the time delay between the target and the antennas. In our experiment, the frequency shift used for calibration is measured by shorting the electrical cables connected to the transmit antenna and the receive antenna. After calibration, the de-chirped frequencies corresponding to Figs. 7(b) and 7(d) are both found to be 4.31 MHz. According to the relationship between the de-chirped frequency and time delay of the radar echo, the distance between the target and the antennas is calculated to be 161.6 cm, with a measurement error of 0.7 cm.

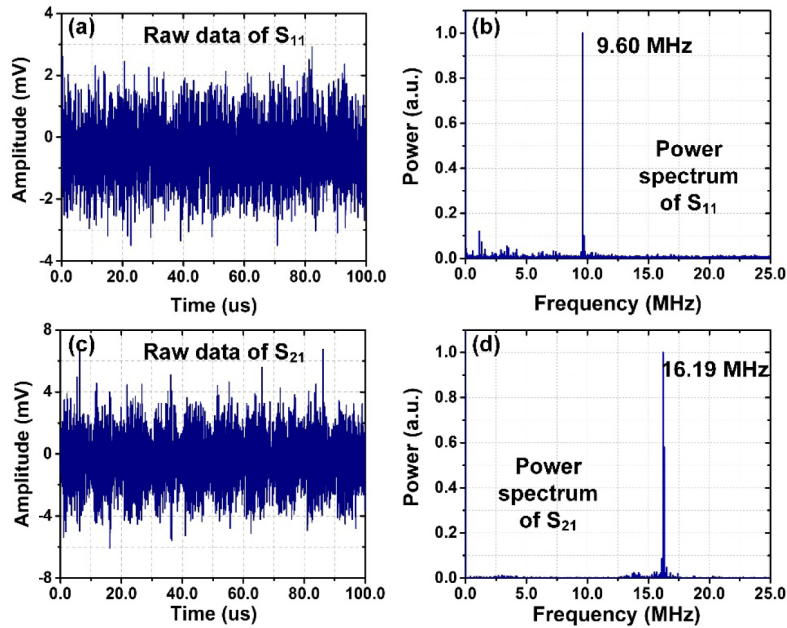


Fig. 7. (a) Waveform and (b) power spectrum of the de-chirped signal  $S_{11}$ , (c) waveform and (d) power spectrum of the de-chirped signal  $S_{21}$ .

The theoretical range-resolution of the MIMO radar, determined by the transmitted signal bandwidth [6], is calculated to be 3.75 cm. To validate this property, detection of two metallic plane targets is implemented, in which the two targets both with a size of about  $6\text{ cm} \times 4\text{ cm}$  are placed about 187 cm away from the antennas. The two targets are separated by 3.75 cm along the range-profile of the radar, as shown in Fig. 8(a). The calculated spectrum of the de-chirped signal  $S_{11}$  is shown in Fig. 8(b), where two de-chirped frequency components at 4.92 MHz and 5.02 MHz are observed. When obtaining the spectrum applying the de-chirped signal  $S_{21}$ , two spectral peaks at 4.92 MHz and 5.02 MHz are also observed. According to the frequencies of these two de-chirped components, the distance between the two targets along the range profile is calculated to be 3.75 cm, which confirms the resolving capability along the range profile.

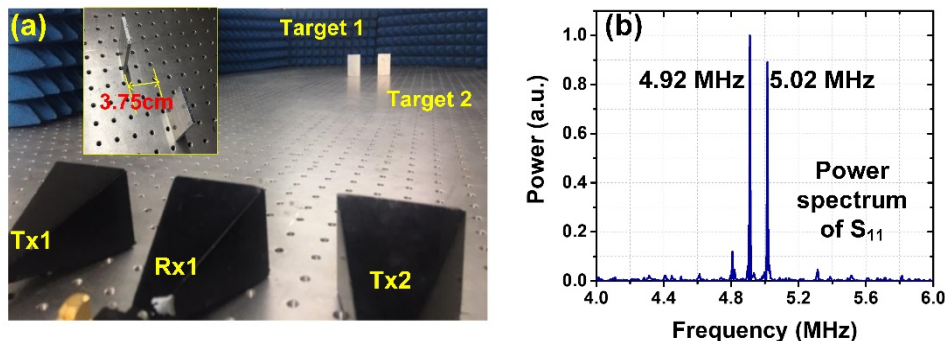


Fig. 8. (a) Picture of the antennas and targets in the experiment, (b) power spectrum of the de-chirped signal  $S_{11}$ .

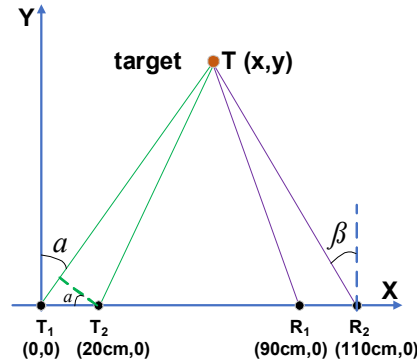


Fig. 9. Illustration of the antennas and target in the Cartesian coordinate when performing the DOA estimation and positioning.

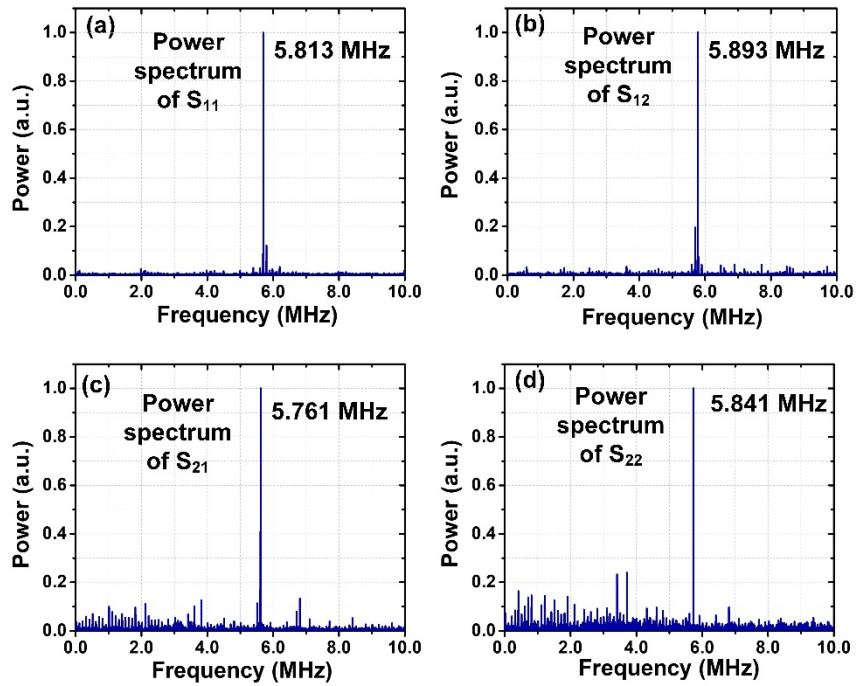


Fig. 10. Calculated power spectra of (a) signal  $S_{11}$ , (b) signal  $S_{12}$ , (c) signal  $S_{21}$ , and (d) signal  $S_{22}$ .

Finally, DOA estimation and target positioning are demonstrated based on the established  $2 \times 2$  MIMO radar. Distribution of the transmit antennas and receive antennas in the Cartesian coordinate is shown in Fig. 9. The two transmit antennas ( $T_1$  and  $T_2$ ) are located at (0, 0) and (20 cm, 0), respectively, and the two receive antennas ( $R_1$  and  $R_2$ ) are located at (90 cm, 0) and (110 cm, 0), respectively. The metallic plane target ( $T$ ) with a size of  $6\text{cm} \times 4\text{cm}$  is arbitrarily placed at (42.5 cm, 212.2 cm). In this case, both the distance between the two transmit antennas and the distance between the two receive antennas are far less than the target distance for the antennas. Thus, Eqs. (3) and (4) are satisfied with the radar parameters. Figure 10 shows the electrical spectra of the four de-chirped signals, where (a), (b), (c) and (d) corresponds to the spectrum of  $S_{11}$ ,  $S_{12}$ ,  $S_{21}$ , and  $S_{22}$ , respectively. Based on the de-chirped frequencies in Fig. 10, the distances corresponding to different paths in Fig. 9 can be

calculated. According to the method in [20], the DOA referenced to  $T_1$ , denoted by  $\alpha$  in Fig. 9, is determined by the following equation,

$$|T_1T_2|\sin(\alpha) = |T_1T| - |T_2T| \quad (5)$$

where  $|T_1T_2|$  is the distance between  $T_1$  and  $T_2$ , and  $|T_1T| - |T_2T|$  is the difference between  $|T_1T|$  and  $|T_2T|$ , which corresponds to the de-chirped frequency difference (0.052 MHz) between  $S_{11}$  and  $S_{21}$ , or between  $S_{12}$  and  $S_{22}$ . By solving Eq. (5),  $\alpha$  is found to be  $11.25^\circ$ . Compared with the real DOA referenced to  $T_1$ , which is  $11.33^\circ$ , the estimation error is  $0.08^\circ$ . Similarly, DOA of the target referenced to  $R_2$ , denoted by  $\beta$  in Fig. 9, is calculated to be  $17.46^\circ$ . Since the real value is  $17.65^\circ$ , the estimation error is  $0.19^\circ$ . Once  $\alpha$  and  $\beta$  are known, the target position can be obtained by solving the following equations

$$\begin{cases} |T_1T| + |TR_2| = \frac{y}{\cos(\alpha)} + \frac{y}{\cos(\beta)} \\ \frac{x}{y} = \tan(\alpha) \end{cases} \quad (6)$$

where  $(x, y)$  is the target position. After solving Eq. (6), the target position is estimated to be (42.52 cm, 213.74 cm), which is separated from the real position by 1.54 cm. Here, the estimation precision is closely related with the accuracy of distance measurement by the established radar, because the DOA estimation in this demonstration is actually realized based on the time of arrival (TOA) estimation. If multiple receivers were applied simultaneously instead of the time-shared receiver in our experiment, the estimation precision could be greatly improved by applying the coherent phase information from multiple receivers [21]. Nevertheless, the DOA estimation and target positioning result are adequate to verify the feasibility of the established photonics-based MIMO radar.

#### 4. Discussion and conclusion

In the experimental demonstration, a 4-GHz bandwidth is adopted to achieve a range resolution of 3.75 cm. While, the photonics-based signal generation and de-chirp processing can easily have a much larger bandwidth over 10 GHz to achieve a higher range resolution [10]. In the receiver, the 100 MSa/s sampling rate can effectively relax the data storage requirement, and it is possible to implement real-time signal processing in real applications. For detection of targets with a large distance, a high de-chirped frequency would be obtained, which may exceed the real-time processing bandwidth. This problem can be solved by either reducing the chirp rate of the transmitted LFM signal, or applying an optical fiber delay line in the reference optical signal to cancel out part of the time delay corresponding to the wireless transmission of the LFM signal [6]. In practice, these solutions may require a priori of the target position. Thus, the proposed MIMO radar is preferred to cooperate with a traditional narrowband radar, which can provide a rough estimation of the target position before acquiring the detailed information by the proposed broadband MIMO radar. It should also be mentioned that the photonics-based broad signal generation and de-chirping make the system more advantageous for a high-frequency MIMO radar because the photonic technologies can overcome the frequency limitations of the state-of-the-art electronics and a higher carrier frequency can help to achieve a higher azimuth resolution. In addition, the photonics-based MIMO radar also has the potential to be incorporated with the fiber-connected communication or sensor networks [22], especially when widely separated antennas are applied. This property may lead to novel applications such as radar-communication fusion and ultra-high resolution remote sensing. Last but not the least, the photonics-based MIMO-ISAR has various applications such as 2D/3D imaging, multi-target detection, and velocity measuring, etc., which are enabled by MIMO radar technology. In

these applications, the involvement of photonic technology is expected to improve the performance and relax the hardware requirements.

A problem with the proposed photonics-based MIMO radar is that, the complexity and cost would increase for a large number of transmitters and receivers, if the radar system is established by discrete devices. This would hinder its practical applications even though much higher performance and more functions can be achieved by the proposed MIMO radar. This problem can be addressed by the integrated microwave photonics technology, because the integration of lasers, detectors, modulators, and other devices such as arrayed waveguide gratings (used as the WDM) on a chip is feasible [23]. Another potential problem is that, to achieve precise parameter estimation, a certain stability of the proposed photonics-based radar is required. For example, when performing DOA estimation via phase difference measurement with the experimental parameters used in our demonstration, a phase difference measurement error of  $\pi/6$  would result in a DOA estimation error over 0.5 degree if the real DOA is less than 30 degree. Therefore, it is preferred that the radar system is operated in a temperature-invariant and vibration-resistant environment, and bias drift problem of the electro-optical modulators is recommended to be addressed by applying bias control circuits. Besides, integration of the system on a chip can also help to improve the stability.

In summary, we have proposed a photonics-based MIMO radar based on wavelength-division-multiplexed broadband microwave signal generation and processing, of which the feasibility is verified through a  $2 \times 2$  MIMO radar with a 4-GHz bandwidth in the transmitter and a 100-MSa/s sampling rate in the receiver. The proposed radar has both the advantages of a photonics-based radar and a MIMO radar, and it is a promising solution for radar applications with both a high resolution and a fast signal processing speed.

### Funding

Natural Science Foundation of Jiangsu Province (SBK2018030017); National Natural Science Foundation of China (NSFC) (61527820); Fundamental Research Funds for the Central Universities (NS2018028).